A Micro Electro-Optical DNA Array Sensor

Samuel Kassegne, Howard Reese, Paul Swanson, Joon M. Yang, Dan Smolko, Dalibor Hodko, Dan Raymond, Marc Madou

Nanogen, Inc., San Diego, CA 92121.

ABSTRACT

We describe a micro electro-optical DNA array sensor whose main features are that it is rapid, sensitive, highly accurate and capable of detecting more than one analyte. These features are the consequence of electronic control of three key elements of DNA assays, namely: concentration of the target molecules at the analysis sites, hybridization of the DNA targets to capture probes and discrimination of complementary DNA from non-complementary DNA. The assays are monitored using a scanning confocal optical platform for fluorescence detection.

A finite-element based computational model for determining electric field distribution at the biochip electrode array and electrophoretic transport of DNA species is built and analyzed. Comparison of theoretical results for electrophoretic DNA accumulation with those obtained from experiments and a simple analytical model is presented.

Keywords: electrochemistry, electric fields, active transportation, sensors, DNA transport, hybridization, micro-mechanical array, finite element analysis, simulation.

1. INTRODUCTION

Detection of DNA molecules in nucleic acid sensors and arrays is commonly achieved by a passive transport of the analyte and/or probe molecules, relying solely on their diffusion to the sensing surface. Often it takes several hours to achieve efficient hybridization of DNA molecules to capture probes or fluorescent probes to the DNA amplicons anchored at the detector surface. This is one of the main impeding factors in making the DNA sensing faster and more accurate within short period of time. We have developed micro electro-optical DNA sensors where transport of biomolecules is achieved through electrokinetic forces [1,2,3,4]. An electrode array covered with a permeation layer with embedded DNA capture probes is used to control the transport of biomolecules and achieve their accumulation and hybridization at the electrodes. The electrode array illustrated in Figure 1 enables both DC and AC electrokinetic manipulation of biomolecules and particles in the detector cell. The array consists of patterned metal electrodes on an insulating substrate and is contained in a plastic housing equipped with fluidic conduits to manipulate sample and other electrolytes. The electrical field applied affects charged analyte biomolecules and particles as well as the ions in the fluid sample.

In the Nanogen's set-up, shown in Figure 1, electrophoresis is used to accumulate the sample onto any of the electrodes in a planar array. The electrodes are covered with a thin layer of hydrogel (permeation layer) and the analyte electrophoreses onto a selected array element through a low conductivity buffer filling the array housing.

Some analyte separation might occur in the thin hydrogel layer but the prime motivation of electrophoresis in this case is to quickly accumulate analyte onto the permlayer. This so-called open electrophoresis technique does not employ small fluidic conduits but closely spaced, individually addressable electrodes on an open chip, as illustrated in Figure 1. This open platform can be exploited to guide and manipulate charged particles such as DNA, RNA, PCR amplicons, polynucleotides, proteins, enzymes, antibodies, nanobeads, and even micron scale semiconductor devices [1,2,3,4]. In dielectrophoresis on the other hand, motion is determined by the magnitude and polarity of charges induced in the particle by an applied field. In electrophoresis, direct current (DC) or low-frequency electric fields, usually uniform, are applied; in dielectrophoresis, on the other hand, alternating current (AC) fields with varying frequencies is used and the field applied is inhomogeneous [5,6,7]. The method is particularly suited for the separation, aggregation, selective trapping, and manipulation and identification of cells and microorganisms [8,9,10]. All types of AC electrokinetics can be carried out on the platform shown in Figure 1 simply by addressing the right set of electrodes in this reconfigurable array. AC electrokinetics was used on the Nanogen platform for cell manipulation and separation and is described elsewhere [11]. The open electrophoresis platform with electrodes across, therefore, has many applications. It enables both DC and AC electrokinetic phenomena and permits larger volume and more complex sample matrix to be used as there are no tiny conduits to be clogged.

In this study, we describe the electric field distribution, the rate of transportation of DNA species to the anode, and compare DNA accumulation obtained through modeling and experiments.

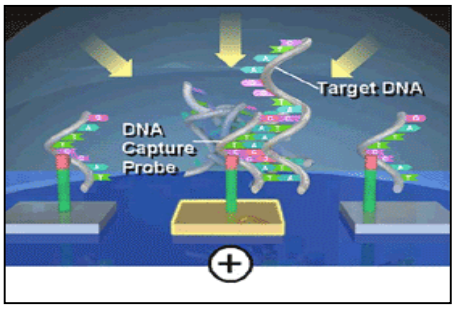

Figure 1. Illustration of DNA transport and hybridization on active electrophoretic DNA chip.

2. DESCRIPTION OF MODEL AND EXPERIMENT

Figure 2 shows the chip geometry used in this study. It consists of a cylindrical flow cell of depth of 500 microns and a diameter of 1000 microns which contains the buffer solution and electrodes. The anode is of 80 micron diameter and has a thickness of 2 microns and is located at the center of the cylindrical flow cell. The cathode is placed at the outer rim of the cylindrical cell and has a width of 40 microns and a thickness of 2 microns. This configuration closely mimics the electrode array chip configuration used in experiments.

The buffer solution is 50mM histidine. A 5 nM concentration of single strand 20 mer DNA (DNA_{20}) sample is used. A constant potential of 1.2 volts is applied at the anode and –0.8 volts is applied at the cathode. This corresponds to a constant voltage used in the experiments with the active DNA array. The valency of the DNA sample is –20 and the DNA's electrophoretic mobility and diffusion constants are assumed to be 15,000 $\mu m^2/v.s$, and 20 $\mu m^2/s$ respectively.

The following assumptions are made in the finite element modeling of the electric field distribution and DNA accumulation in the active DNA micro array:

1. The effect of pH change on the ensuing chemical reactions due to generation of hydrogen and hydroxyl ions is neglected. Earlier studies suggest that pH changes in histidine buffer are within the range of 6.5 to 6.0 [12], suggesting a negligible effect.
2. The effect of the charges carried by the DNA species on the electric field is neglected.
3. The effect of permeation layer on the DNA transport and accumulation and electric field distribution is neglected.
4. The effect of diffusion is included.

Two modeling approaches are pursued in this study, i.e., a 3D finite element analysis and a simplified analytical model. The finite element analysis (FEA) was carried out using the CoventorWare™ software from Coventor, Inc while the simplified analytical model is based on a simple relationship between the current carried by DNA species and the total current in the chip, as described in Equations (1.a – 1.c).

The finite element simulation consisted of a finite element (FE) mesh for a two-dimensional slice of the flow-cell with 1395 8-noded parabolic elements and a total number of 6108 nodes, as shown in Figure 3. This mesh was selected after a convergence study on current density and electric field distribution. The FE mesh, as expected, is much more dense at the location of the electrodes due to the sharp corners in the geometry and also due to the high gradient of electric field and current density at these locations. At locations further from the electrodes, the mesh is noticeably coarse resulting in saving of computational time.

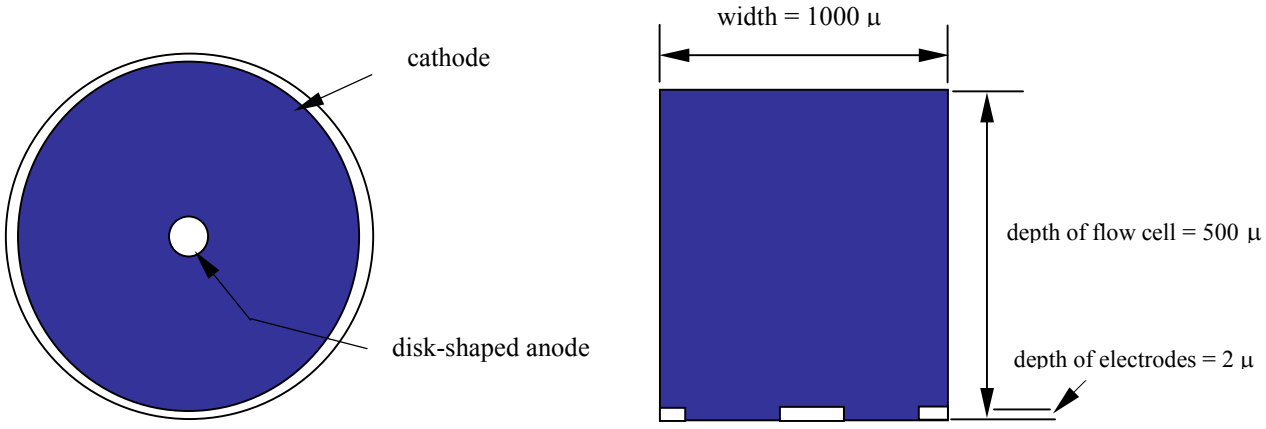

a) plan view of a ring electrode chip in a cylindrical flow cell b) side view of the cylindrical flow cell

Figure 2. Geometry of a ring electrode system in a cylindrical flow cell.

The sample used for the experimental accumulation studies was a 50 nM solution of a fluorescently labeled T12 oligonucleotide in 50 mM histidine. 10μl of this sample was placed on a 25-site micro-array coated with an agarose/streptavidin permeation layer. One of the array sites was addressed at a constant current setting of 1μA for

60 seconds. The accumulation of fluorescence over the array site was monitored during the 60 second address. The resulting fluorescence signal was quantified by comparison to fluorescent standards of known concentration.

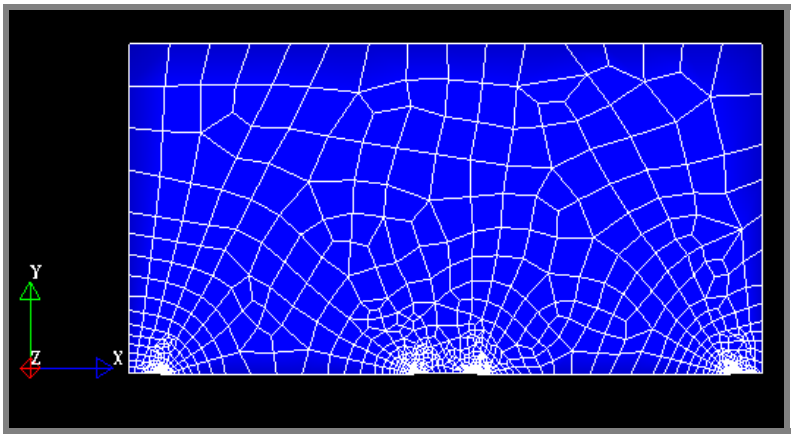

Figure 3. Finite element mesh of a 2D model of a cylindrical flow cell.

The analytical model that gives the number of DNA species accumulated on the anode within time, 't' can be derived as follows:

$$\boldsymbol{J}_{DNA} = (\sigma_{DNA}/\sigma)\, J \qquad \text{Equation (1.a)}$$

where,

$\boldsymbol{J}_{DNA}$ is that part of the current carried by DNA species and J is the total current in the chip,
σ is conductivity of the buffer solution, and
σ_{DNA} is the conductivity of DNA and can be expressed as:

$$\sigma_{DNA} = z\, e\, n\, \mu = z\, c\, F\, \mu \qquad \text{Equation (1.b)}$$

Equation (1.a) can be re-written as:

$$N_{DNA} = (J_{DNA} / z\, e)\, t = (F\mu/e\sigma)\, cJt \qquad \text{Equation (1.c)}$$

where,

F is Faraday constant,
μ is the electrophoretic mobility of DNA,
e is the charge carried by a single electron,
c is the concentration of DNA,
Z is the number of charges on the DNA, and
t is time in seconds.

3. SIMULATION AND RESULTS

This section presents some of the important numerical results obtained from the simulation of the electrochemical cell. The key quantities of interest covered in this study are, electric field distribution, transport and accumulation of DNA species.

The transport of DNA species in the flow cell in the active DNA array sensor depends primarily on the electric field distribution. The electric field is dense at both the anodes and cathodes. It is in these regions, therefore, where transport of DNA species is highest. Figure 4 shows the electric field distribution with regions of dense electric fields clearly established within the vicinity of electrodes. These regions are at the anode which is located at the middle and at the cathode which is located at the edges. Further, note that, depth-wise, the electric field is very sparse in the areas far away from the electrodes suggesting that the electric field distribution decreases quite fast in the depth direction. The radial distribution of the electric fields is plotted in Figure 5 with clear peaks at the anode and cathode. A closer look at Figure 5 will further reveal that the electric fields are highest at the corner of the anode and cathode. Consequently, we expect greater accumulation of DNA at the corners of the anode. This is also indeed observed in our experiments.

With respect to species transportation, as soon as electric field is applied to the electrodes, DNA starts moving to the anodes where it is accumulated. At the cathode, DNA is repelled due to its negative polarity. Figure 6 shows the variation of accumulation of DNA (i.e., total DNA flux) at the surface of the anode with respect to time. The x-axis gives the change in time whereas the total DNA flux is given in the y-axis. The DNA influx at the anodes was followed for 150 seconds at which time an onset of saturation was observed. The transport of DNA is also indicated in Figure 7 which shows species transport as a moving front at time t = 30 seconds. Note that expulsion of DNA species from the cathodes is indicated by the same figure by lighter shades.

The result of DNA accumulation was compared with experimental results and a simplified analytical model. The comparison is given in Table 1 which demonstrates that the finite element analysis (FEA) simulation gives, for practical purposes, a good comparison of accumulation rate with the simple analytical model and the experimental results. However, it has to be noted that the analytical model used in the comparison does not consider diffusion which could be significant.

	C_{DNA}			
	T = 10 Sec	30 Sec	60 Sec	90 Sec
Experimental Result	< 1%	< 1%	1%	--
Analytical Model	< 1%	0.9 %	1.8%	2.6%
FEA Model	< 1%	1.2 %	2.5%	3.5%

Table 1. Comparison of DNA accumulation results from experiments and numerical models.

The FEA simulation discussed here, however, does not model the chemistry of the histidine buffer where such effects as the consumption of H^+ ions by histidine, and the generation of hydrogen and hydroxyl ions could introduce change in pH which in turn will affect the analyte and species transport properties in the flow cell. While a previous study [12] suggested negligible pH changes in histidine buffers, the total effects due to bulk chemical reactions that result in generation of ions, however, need further investigation.

The results from finite element analysis, experiment and analytical model confirm that indeed the electrophoretic accumulation of DNA occurs within few seconds and minutes, as compared to passive hybridization which sometimes could take hours. Table 1 also demonstrates that by increasing the accumulation time, significantly higher concentration of DNA is achieved at the anode. This result provides a basis for optimizing the DNA accumulation time with respect to the number of electrodes addressed and the targeted detection limits.

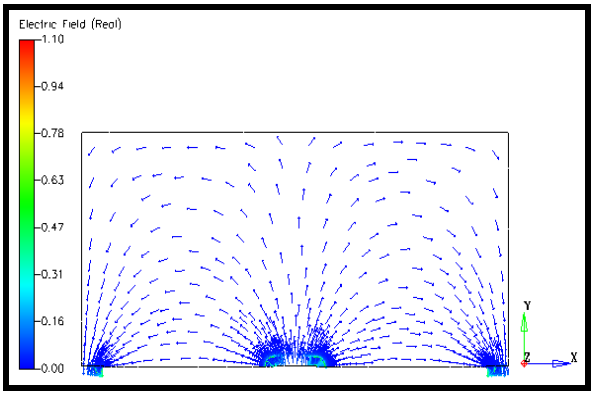

Figure 4. Electric field distribution in the flow cell.

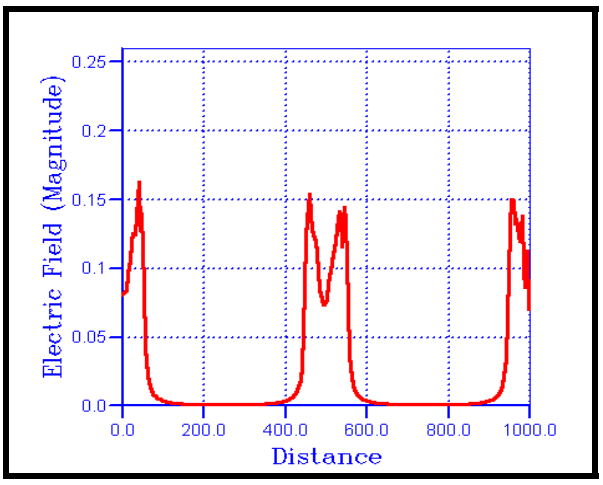

Figure 5. Radial distribution of electric field distribution.

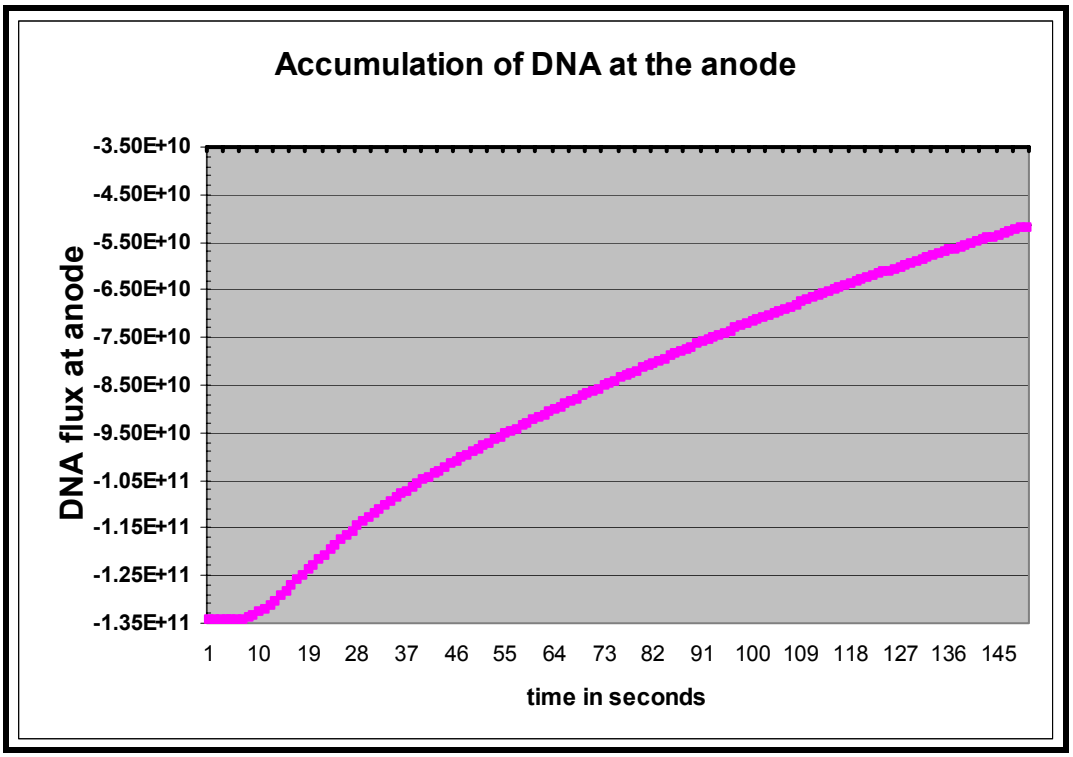

Figure 6. Accumulation of DNA at the anode with respect to time.

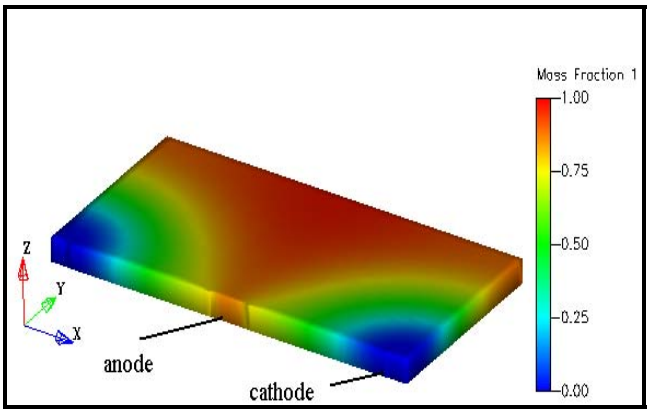

Figure 7. Transport of DNA species shown as a moving front between the cathode and anode.

1. CONCLUSIONS

This study demonstrates the simulation of the transport and accumulation phenomenon in an active DNA biochip array. Important quantities such as radial and depth-wise electric field distribution, DNA species transport and accumulation are modeled and their results compared with experimental findings and a simplified analytical model. The simulations indicated that understanding the electric field distribution, the driving force for electrophoretic

DNA transport is crucial for the cell design and optimizing DNA accumulation at the electrodes. The finite element analysis modeling included the effect of diffusion which cannot be ignored if close correlation with experimental results is intended. Both experimental and modeling results confirmed that electronic addressing of DNA at the electrodes offers substantial advantages compared to passive hybridization controlled solely by diffusion. DNA accumulation is achieved within seconds at a locus of fluorescence detection. The modeling results were in close correlation with the experimental results, providing a design tool for optimizing the conditions for accumulation of DNA with respect to electric field applied, time of accumulation, targeted detection sensitivity, and the number of electrodes or detection loci.

ACKNOWLEDGEMENTS

We would like to acknowledge the contribution of Lei Wu in his work on the simple analytical model presented here.

REFERENCES

1. Edman, C.F., Swint, R.B., Gurtner, C., Formosa, R.E., Roh, S.D., Lee, K.E., Swanson, P.D., Ackley, D.E., Coleman, J.J., Heller, M.J.*, "Electric Field Directed Assembly of an InGaAs LED onto Silcon Circuitry", IEEE,* Vol.12, No.9: 1198-1200 , September 2000.
2. Radtkey, R., Feng, L., Muralhider, M., Duhon, M., Canter, D., DiPierro, D., Fallon, S., Tu, E., McElfresh, K., Nerenberg, M. and Sosnowski, R., "*Rapid high fidelity analysis of simple sequence repeats on an electronically active DNA microchip",*. Nucleic Acids Research , January 2000.
3. Eugene Tu, Anita H. Forster, Michael J. Heller, "*Active microelectronic chip devices which utilize controlled electrophoretic fields for multiplex DNA hybridization and other genomic applications*", *Electrophoresis 2000*, 21, 157-164, 2000.
4. Cheng, J., Sheldon, E.L., Wu, L., Uribe, A., Gerrue, L.O., Carrino, J., Heller, M., and O´Connell, J, "*Electric field controlled preparation and hybridization analysis of DNA/RNA from E. coli on microfabricated bioelectronic chips*", Nature Biotechnology*,* 16: 541-546 , 1998.
5. Pohl, H.A *Dielectrophoresis*; Cambridge University Press: Cambridge, UK, 1978.
6. Jones, T. B, *Electromechnics of Particles*; Cambridge University Press: Cambridge, UK, 1995.
7. Pethig, R., *Crit Rev Biotechnol* 16: 331-348, 1996.
8. Wang X. B, Huang Y, Hölzel R, Burt JPH, Pethig R, J Phys D: Appl Phys 26: 1278-1285, 1993.
9. Markx G.H, Huang Y, Zhou XF, Pethig R., Microbiology 140: 585-591, 1994.
10. Cheng J, Sheldon E.L, Wu L, Heller MJ, O'Connell JP., JP Anal Chem 70: 2321-2326, 1998.
11. Huang Y.K, Ewalt L, Marcus T, Haigis R, Forster A, Ackley D, Heller MJ, O'Connell JP, Krihak M, Anal Chem 73: 1549-1559, 2001.
12. Edman, F.E., Raymond, D.E., Wu, D.J., Tu, E., Sosnowski, R.G., Butler, W.F., Nerenberg, M., and Heller, M.J., "Electric field directed nucleic acid hybridization on microchips", Nucleic Acids Research, Vol. 25, No 24, 1997.